JACS
JOURNAL OF THE AMERICAN CHEMICAL SOCIETY

Article

pubs.acs.org/JACS

# Control of the Redox Activity of PbS Quantum Dots by Tuning Electrostatic Interactions at the Quantum Dot/Solvent Interface

Chen He, David J. Weinberg, Alexander B. Nepomnyashchii, Shichen Lian, and Emily A. Weiss*

Department of Chemistry, Northwestern University, 2145 Sheridan Rd., Evanston, Illinois 60208-3113, United States

Supporting Information

**ABSTRACT:** This paper describes the control of electron exchange between a colloidal PbS quantum dot (QD) and a negatively charged small molecule (9,10-anthraquinone-2-sulfonic acid sodium salt, AQ), through tuning of the charge density in the ligand shell of the QD, within an aqueous dispersion. The probability of electron exchange, measured through steady-state and time-resolved optical spectroscopy, is directly related to the permeability of the protective ligand shell, which is a mixed monolayer of negatively charged 6-mercaptohexanoate (MHA) and neutral 6-mercaptohexanol (MHO), to AQ. The composition of the ligand shell is quantitatively characterized by $^1$H NMR. The dependence of the change in Gibbs free energy, $\Delta G_{obs}$, for the diffusion of AQ through the charged ligand shell and its subsequent adsorption to the QD surface is well-described with an electrostatic double-layer model for the QD/solvent interface. Fits of the optical data to this model yield an increase in the free energy for transfer of AQ from bulk solution to the surface of the QD (where it exchanges electrons with the QD) of 154 J/mol upon introduction of each additional charged MHA ligand to the ligand shell. This work expands the set of chemical parameters useful for controlling the redox activity of QDs via surface modification and suggests strategies for the use of nanoparticles for molecular and biomolecular recognition within chemically complex environments and for design of chemically stable nanoparticles for aqueous photocatalytic systems.

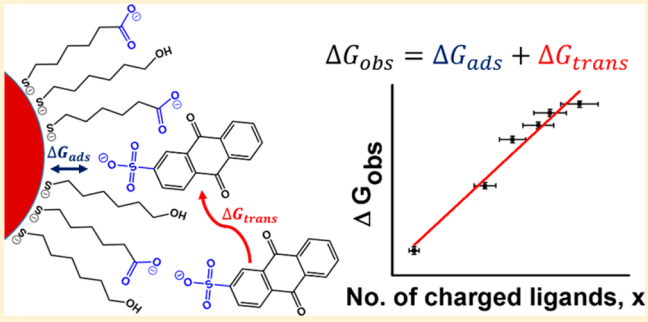


## INTRODUCTION

This paper describes the relationship between a controlled electrostatic charge density within the organic adlayer of a colloidal PbS quantum dot (QD) and the permeability of that adlayer to a negatively charged small molecule, 9,10-anthraquinone-2-sulfonic acid sodium salt (AQ, Figure 1A). We coat the PbS QDs with mixed monolayers of neutral ligands (6-mercaptohexanol, MHO) and ligands with a negatively charged tail group (6-mercaptohexanoate, MHA), Figure 1B, and change the ratio of MHO to MHA within the monolayer to tune the Coulomb repulsion between the outer surface of the ligand shell and the charged sulfonate substituent on AQ. These nanoscale electrostatic interactions control the permeability of the ligand shell to AQ and the probability of photoinduced electron transfer (eT) from the QD to AQ. The relationship between the yield of eT and the number of charged ligands at the QD surface is well-described by an electrostatic double-layer model, which yields a value for the contribution of each added charge to the free energy for permeation of AQ through the ligand shell of 154 J/mol.

Colloidal QDs, synthesized with wet chemical methods, form a class of highly versatile, solution-processable nanoscale building blocks for bottom-up fabrication of hierarchical structures with widespread potential applications, such as solid-state electronics,[1,2] solar cells,[3,4] photocatalysts,[5,6] and biological tags.[7−9] The performance of QDs in any of these applications depends on controlling their interactions with small molecules and ions that, for example, quench their photoluminescence (PL) through charge or energy transfer, corrode their surfaces through reactions with surface ions or ligands, or induce aggregation of particles. One method for maximizing the interaction of QDs with specified molecules and minimizing nonspecific interactions is to use the self-assembled monolayer (SAM) that serves as the ligand shell for the QD as a semipermeable membrane (much like their analogues on planar surfaces)[10,11] and, ultimately, a molecular recognition layer.[12−15] An important technique to create selectively permeable membranes is to make them electrically charged. The density and type of these charges control the electrostatic potential at the membrane-solvent interface and have been reported to gate the rate of interfacial reactions on a planar electrode[16−18] and control the efficiency of ion transport through a cylindrical nanopore.[19,20]

We choose colloidal QDs as our experimental system because (i) the sensitivity of the dynamics of the QD's excited state (exciton) to proximate molecules allows us to use optical spectroscopy to measure the degree of permeation of these molecules through the ligand shell, and (ii) control of the redox activity of QDs and the chemical stability of QD surfaces in

**Received:** April 18, 2016
**Published:** June 24, 2016





DOI: 10.1021/jacs.6b03970
J. Am. Chem. Soc. 2016, 138, 8847−8854

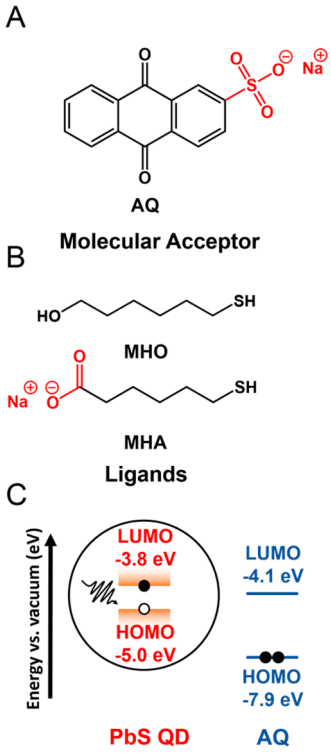


**Figure 1.** (A) Structure of AQ, the electron acceptor. (B) Structures of the MHO and MHA ligands that solubilize the PbS QDs in aqueous solution. (C) Frontier orbital energies (vs vacuum) of the PbS QD ($R$ = 1.6 nm) and AQ. The LUMO of AQ was measured with cyclic voltammetry, and the HOMO energy equals the LUMO energy minus the optical bandgap. Electron transfer from the photoexcited QD to AQ has a driving force of −0.3 eV, while hole transfer and energy transfer are energetically uphill.

aqueous environments using surface functionalization is a prerequisite to the development of a selective molecular recognition, drug delivery, or photocatalytic systems based on QDs.

Measurement of the yield of photoinduced eT between the QD and AQ is a sensitive probe of adlayer permeability. The yield of eT upon mixing, for example, 200 molar equiv of AQ with the QDs ranges from 10% at a charge density of 1.1 charges/nm$^2$ to 98% at a charge density of 0.29 charges/nm$^2$ (see the Supporting Information, Table S6). The basis of this technique is that eT between a QD and a small molecule acceptor does not occur on a time scale competitive with other relaxation mechanisms of the QD unless the small molecule has permeated through the ligand shell and is at (or very near) the inorganic surface of the particle.[12,15,21−26] The probability of eT is therefore directly correlated with the probability of permeation. The use of photoinduced interfacial eT, rather than cyclic voltammetry (which is commonly used to probe the structure of monolayers on planar metal and metal nanoparticles[27,28]) for this measurement is necessary because applied static potentials typically induce irreversible redox processes on QD surfaces, whereas eT from the photoexcited state of the QD is reversible and nondestructive.

This work is a first step toward designing monolayers on photoactive, electroactive semiconductor QDs for nanoscale molecular recognition based on electrostatic interactions.

## RESULTS AND DISCUSSION

**Synthesis of Water-Soluble PbS QDs.** Oleate-capped PbS QDs with a first excitonic peak at ∼985 nm and radius of 1.6 nm[29] were synthesized using a procedure adapted from that of Hines and Scholes,[30] see the Supporting Information. We prepared water-soluble PbS QDs capped with mixed monolayers of 6-mercaptohexanoate (MHA) and 6-mercaptohexanol (MHO) through ligand exchange using a method adapted from those of Hyun et al.[31] and Kalsin et al.[32] We added 400 equiv of thiols per QD in total, with various MHO/MHA ratios, to a 5 mL sample of 40 $\mu$M oleate-capped PbS QDs dispersed in $CHCl_3$ and shook the mixture rigorously for 1 min until the QDs flocculated. We then added between 96 and 480 equiv of NaOH per QD (NaOH/MHA = 1.2:1) to the mixture to deprotonate the −COOH groups ($pK_a \approx 4.8$)[33,34]) and make the QDs negatively charged and water-soluble. The QDs precipitated out of solution as we added NaOH and transferred to the aqueous layer as we added 4 mL of water on top of the chloroform and gently shook the mixture. We then centrifuged this mixture at 7000 rpm for 10 min to facilitate the separation between aqueous and organic layers, which are sometimes emulsified due to the presence of surfactants. The optically clear aqueous layer was separated and washed with 10 mL chloroform to eliminate displaced oleate species, and this aqueous layer served as a stock solution of MHA/MHO-capped PbS QDs. The range of pH for all QD samples (2.63 $\mu$M) we investigated was 9.6−10.3. $^1$H NMR spectra of the aqueous QD dispersions show that all the oleate ligands that were initially bound to the QDs are displaced upon addition of 400 equiv of thiols, see the Supporting Information, Figure S3.

**Quantification of MHA/MHO Mixed-Monolayer Ligand Shell.** We prepared water-soluble PbS QDs capped with mixed monolayers of MHO/MHA of six different compositions using the procedures described above and determined their concentrations from the intensity of their ground-state absorption spectra at 400 nm.[29] We then prepared a 13.2 $\mu$M sample of each type of QD in $D_2O$ and quantified the compositions of the ligand shells of the QDs in each sample by $^1$H NMR spectroscopy, with 800 equiv of sodium formate added as the internal integration standard (sharp singlet at 8.33 ppm, 1H, see the Supporting Information, Figure S3A). We set the acquisition time to 27 s and the relaxation time to be 90 s to allow for complete collection of FID signal and sufficient relaxation of $^1$H nuclei between measurements, performed 8 scans of each sample (except for samples 5 and 6, for which we took 32 scans in order to improve the S/N ratio), and used a sum of 5 Lorentzian functions to fit the acquired spectra. Figure 2 contains representative spectra of these samples in the region of interest; the full set spectra are in the Supporting Information, Figures S3A and S5.

The NMR spectra of the MHO/MHA-capped QDs contain a broad peak centered at ∼2.07 ppm corresponding to the protons alpha to the $-COO^-$ in bound MHA[35,36] and a sharp triplet centered at ∼2.03 ppm corresponding to those protons on freely diffusing MHA. A weak singlet at ∼2.08 ppm is assigned to an unknown impurity; the intensity of this peak does not scale with the concentration of MHA, and we subtract this feature from the spectrum before integrating any peaks. The total number of MHA (bound plus free) per QD in solution is calculated by integrating the portion of the spectrum containing both peaks. In order to deconvolute the bound and free MHA signals, we integrate the broad feature (the red fitting


DOI: 10.1021/jacs.6b03970
J. Am. Chem. Soc. 2016, 138, 8847−8854

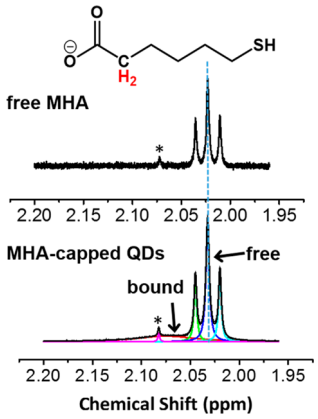


**Figure 2.** $^1$H NMR spectra of MHA molecules in $D_2O$ (top) and sample 1 (see Table 1) of MHA-capped PbS QDs in $D_2O$ (bottom), showing signals from the highlighted methylene group (red). The spectrum of the QDs is fit with a sum of five Lorentzian functions with component peaks shown in different colors. The sharp triplet at ∼2.03 ppm corresponds to free MHA ligands, while the broad feature centered at ∼2.07 ppm (the red fit line) corresponds to MHA ligands bound to the surface of QD. The small singlet at ∼2.08 ppm, marked by asterisk (*), originates from an impurity in $D_2O$ solvent; its intensity does not scale with the absolute concentration of MHA ligands in the sample.

line in Figure 2) and sharp triplet from 1.96 to 2.20 ppm separately against the sodium formate internal standard and assign these two numbers as the number of bound and free MHA per QD, respectively. Table 1 lists the results of our

**Table 1. Compositions of the Mixed Organic Adlayers of MHA/MHO-Capped PbS QDs**

| no. of sample | equiv of MHA/MHO added to PbS QDs | equiv of MHA (bound + free) measured[a,b] | equiv bound MHA measured ($x$)[a,c] | equiv free MHA measured[a,d] | equiv bound MHO estimated[a,e] |
|---|---|---|---|---|---|
| 1 | 400/0 | 438 ± 36 | 115 ± 9 | 323 ± 27 | 0 |
| 2 | 320/80 | 311 ± 26 | 100 ± 8 | 210 ± 17 | 80 |
| 3 | 280/120 | 286 ± 24 | 94 ± 8 | 192 ± 16 | 116 ± 8 |
| 4 | 240/160 | 263 ± 22 | 81 ± 7 | 182 ± 15 | 139 ± 7 |
| 5 | 160/240 | 170 ± 14 | 67 ± 6 | 104 ± 9 | 153 ± 6 |
| 6 | 80/320 | 86 ± 7 | 31 ± 3 | 55 ± 5 | 189 ± 3 |

[a]The errors are propagated from systematic error in the NMR measurement using the calibration plot described in the Supporting Information, Figure S12. [b]Calculated from the sum of the bound (∼2.07 ppm, broad feature) and free (∼2.03 ppm, sharp triplet) MHA signals. [c]Calculated from the broad feature centered at ∼2.07 ppm. [d]Calculated from the triplet centered at ∼2.03 ppm. [e]Estimated as (220 − no. of bound MHA). If fewer than (220 − no. of bound MHA) MHO ligands were added, equiv of MHO bound = equiv of MHO added.

quantitative NMR analysis for all six samples of MHA/MHO-capped PbS QDs with different mixed monolayer compositions. We note that the total number of MHA ligands per PbS QD, as measured by NMR, is in a few cases slightly (up to 9.6%) larger than the total equivalents of MHA we added, a discrepancy that can be accounted for by (i) the systematic error of our NMR measurement (∼+8%, see the calibration curve in the Supporting Information, Figure S12), and (ii) incomplete phase transfer: up to 15% of oleate-capped QDs, either unreacted or only partially exchanged by MHA, are not present in the final aqueous solution (see the Supporting Information, Table S1), which increases the MHA:QD ratio.

The number of MHO ligands bound per QD is more difficult to determine from their NMR spectra, because the MHO molecules are in fast exchange with the QD surface and therefore present a single broad feature at ∼3.5 ppm (see the Supporting Information, Figure S6). We estimate the number of bound MHO ligands per QD by subtracting the number of bound MHA ligands per QD (measured as described above) from 220, the total number of thiol binding sites per QD, which we measured by titrating the oleate-capped QDs with hexanethiol and counting the number of displaced oleates (see the Supporting Information, Figure S4). This method of ligand counting is indirect, but only the number of bound MHA per QD (and not the number of bound MHO per QD) determines the charge density at the QD surface, so the absolute number of MHO per QD is not critical to the analysis that follows. There are no detectable oleate ligands bound to the surfaces of the QDs after phase transfer, see the Supporting Information, Figure S3B.

**Photoinduced Electron Transfer Occurs from PbS QDs to Adsorbed AQs.** We added a series of equivalents of AQ (20 equiv − 6000 equiv), which has one negative charge on its sulfonate group ($pK_a \approx -1.8$)[33] as shown in Figure 1A, to 2.63 $\mu$M of PbS QDs and allowed all of the samples to sit in the dark for 4 h to equilibrate, as indicated by a saturation in the PL of the QDs, see the Supporting Information, Figure S8. The PL of the QDs decreased monotonically with increasing equivalents of AQ added, Figure 4A. Based on the electrochemical potentials of AQ and the measured conduction and valence band-edges of PbS QDs of this size, measured using photoemission spectroscopy,[37] Figure 1C, eT from the conduction band-edge (or LUMO) of the QD to the LUMO of AQ is the most likely mechanism for quenching of the QDs' PL. Electron transfer has a driving force of −0.3 eV, but both hole transfer and energy transfer from the QD to AQ are energetically uphill and do not occur.

Transient absorption (TA) measurements on the QD/AQ mixtures confirm that the PL quenching upon addition of AQ is due to photoinduced eT from the QD to AQ. We performed TA on the picosecond-to-nanosecond time scale on two samples of QDs with different surface compositions, one with QDs capped with 115 MHA/QD (sample 1) and one with QDs capped with 31 MHA/QD (sample 6), each mixed with two different concentrations of AQ, as shown in Figure 3A,B. We also performed the same measurements for these two QD samples with no added AQ. The setup for the TA experiment and the protocols for fitting these data are detailed in the Supporting Information. The inset of Figure 3A shows a representative TA spectrum of 115 MHA-capped PbS QDs, at 2 ps after excitation with a 850 nm pump pulse. The large negative feature is the ground state bleach, and we monitor its evolution in time to measure the dynamics of exciton decay in the absence and presence of AQ. Figure 3A,B shows these dynamics on the picosecond-to-nanosecond time scale for the QDs with different surface compositions (the corresponding PL spectra of these samples are in the Supporting Information, Figure S10). Addition of AQ to the QDs induces additional decay pathways on the 100 ps time scale (see the Supporting Information, Table S3A), and this new decay gets faster (and results in a larger bleach recovery) as the number of equivalents of AQ increases. These observations are consistent with the PL quenching data (Figure 4A) and are characteristic of


DOI: 10.1021/jacs.6b03970
J. Am. Chem. Soc. 2016, 138, 8847−8854

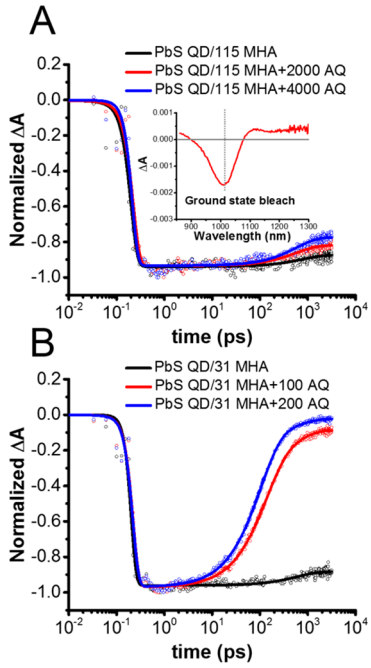


**Figure 3.** (A) Normalized kinetic traces extracted at the ground-state bleach (1014 nm, inset) from the TA spectrum of a 6.58 $\mu$M sample of 115-MHA capped PbS QDs mixed with 0 equiv (black), 2000 equiv (red) and 4000 equiv (blue) of AQ. (B) Normalized kinetic traces extracted (at 1039 nm) from the TA spectrum of a 6.58 $\mu$M sample of 31 MHA-capped PbS QDs mixed with 0 equiv (black), 100 equiv (red), and 200 equiv (blue) of AQ. The solid lines in A and B are multiexponential fits of the traces with parameters summarized in Table S3A in the Supporting Information.

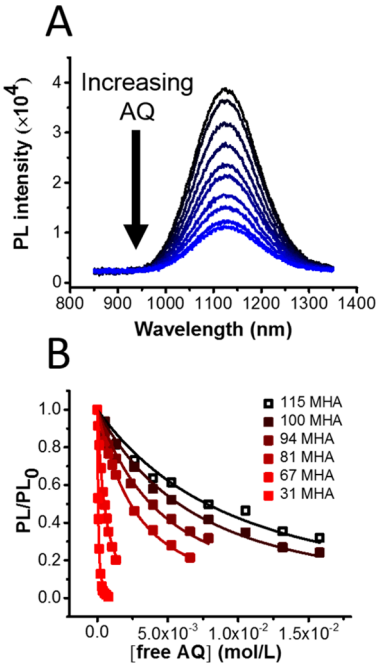


**Figure 4.** (A) PL spectra of sample 1 (see Table 1), 2.63 $\mu$M PbS QDs each capped by 115 MHA ligands, mixed with increasing equivalents of AQ. The decreasing intensity of PL indicates a growing eT yield as we increase the number of electron acceptors adsorbed per QD. (B) Plot of $PL/PL_0$, the fraction of originally emissive QDs that remain emissive after addition of AQ, vs concentration of free AQ in solution, fit using eq 4. The lower the surface coverage of the negatively charged MHA ligand on the QDs, the more efficiently AQ quenches the PL of the QDs. The PL quenching for the sample of the QDs capped with 115 MHA ligands (shown in open symbols) has a contribution from collisional eT between freely diffusing species, in addition to the quenching within static QD−AQ complexes, see the Supporting Information, Table S3B.

depopulation of the excited state by eT from the exciton of the QD to the LUMO of statically adsorbed AQ, as we and others have seen for many QD-molecule combinations.[12,15,24,38−42] As we and others have reported, the observed rate constant for eT scales linearly with the number of adsorbed molecular acceptors.[12,24,41−43] In this work, the intrinsic eT rate within each QD-AQ pair was calculated to be $2.4 \pm 0.2 \times 10^9$ $s^{-1}$ from fitting a plot of the observed eT rate vs the number of bound AQs, $\lambda$, with a line (see the Supporting Information, Figure S11).

**The Yield of Photoinduced Electron Transfer Is a Probe of the Permeability of the Charged Organic Adlayer to AQ.** Figure 4B contains plots of the ratio $PL/PL_0$, the fraction of emissive QDs in a sample that remain emissive after addition of AQ, vs the concentration of free AQ in the sample, for QDs with the six surface compositions that we studied with NMR. For a given concentration of added AQ, $PL/PL_0$ increases with increasing coverage of the charged MHA ligand; therefore, the yield of eT to the charged AQ molecule (which is inversely proportional to $PL/PL_0$) decreases with increasing negative charge density on the QD surface. This conclusion is supported by the data in Figure 3A,B, which show that exciton decay is accelerated much more dramatically in the QDs with fewer surface charges, despite the fact that more highly charged QDs were mixed with a factor of 20 more AQ than the less-charged QDs. This decrease is not due to a change in the energetics of the charge-transfer reaction (changing the density of charges that are more than 1 nm from the QD surface has a negligible effect on the energy of the photoexcited electron), but rather reflects a decrease in the average number of AQ molecules adsorbed to each QD surface, i.e., the number of donor−acceptor complexes formed. The probability of forming a QD-AQ donor−acceptor complex is related to the permeability of the MHA/MHO ligand shell to AQ.

In order to use these PL quenching data to define the relationship between the surface charge density of the QD and its permeability to the charged AQ electron acceptor, we need a model for the probability of binding of AQ to the QD surface as a function of this charge density. Assuming that the binding of each AQ occurs with a probability that is independent of previous binding events, the probability of finding a QD with $n$ AQs absorbed to its surface can be described by a Poisson distribution, eq 1,[12,25,41,44,45] where $\lambda$ is the mean number of AQs bound per QD in the

$$p(n, \lambda) = \frac{\lambda^n}{n!} e^{-\lambda} \quad (1)$$

ensemble. We then assume that adsorption of an AQ to a QD quantitatively quenches the PL of that QD, because the time scale of eT, measured by TA (100−600 ps), is a factor of 4−16 $\times 10^3$ faster than the exciton lifetime of the QD. With this assumption, $PL/PL_0$, the fraction of QDs that remain emissive after addition of AQ, equals the probability of finding a QD with zero adsorbed AQ molecules: $PL/PL_0 = p(n = 0)$.

We combine this definition of $PL/PL_0$ (a measurable quantity) with eq 1 to yield eq 2:


DOI: 10.1021/jacs.6b03970
J. Am. Chem. Soc. 2016, 138, 8847−8854

$$\lambda = -\ln\left(\frac{PL}{PL_0}\right) \tag{2}$$

an expression for $\lambda$. $\lambda$ can also be described by the Langmuir isotherm, eq 3a, where $K_a$ is the

$$\lambda = \lambda_{max} \times \frac{K_a[AQ]_{free}}{1 + K_a[AQ]_{free}} \tag{3a}$$

equilibrium adsorption constant for the PbS QD−AQ complex at 298 K, and the concentration of free AQ in aqueous solution is determined by subtracting the number of bound AQ from the number of added AQ, eq 3b:

$$[AQ]_{free} = [AQ]_{added} - \lambda[QD] \tag{3b}$$

We combine eqs 2, 3a, and 3b to yield eq 4, which relates $PL/PL_0$ to $[AQ]_{free}$:

$$\frac{PL}{PL_0} = e^{-\lambda_{max} \times K_a[AQ]_{free}/(1+K_a[AQ]_{free})} \tag{4}$$

, and use this equation to globally fit the data in Figure 4B with a shared value of $\lambda_{max}$ (the maximum number of AQ binding sites per QD) for all six data sets. We shared $\lambda_{max}$ across all of the samples in order to further constrain our fit and minimize codependence between $\lambda_{max}$ and $K_a$. This constraint is physically reasonable because, with the presence of excess thiolate (MHA and MHO) ligands in solution, all samples of PbS QDs should have the same total number of bound ligands (~220, except for sample 1), and it is this ligand density that determines the number of available binding sites for AQ. Table 2 lists the values of the parameters extracted from these fits. We find that $\lambda_{max}$ = 4.7 per QD, which agrees with a previously reported study of the binding of aminoferrocene to PbS QDs of similar size.[15] As we decrease the average number of bound MHA from 115 per QD to 31 per QD, the apparent $K_a$ for the PbS-AQ system increases from $2.2 \times 10^1$ $M^{-1}$ to $3.2 \times 10^3$ $M^{-1}$. For convenience, we apply eqs 5a and 5b[46] to translate $K_a$ first into

**Table 2. Maximum Surface Coverage, $\lambda_{max}$, Equilibrium Constants, $K_a$, and Corresponding Gibbs Free energy change, $\Delta G_{obs}$, for Adsorption of PbS QD−AQ Complexes with Different QD Surface Compositions**

| no. of sample | no. of (−) charges per QD ($x$)[a] | no. of AQ binding sites per QD ($\lambda_{max}$)[b] | $K_a$[b] for QD−AQ complex ($M^{-1}$) | $\Delta G_{obs}$[c] for formation of QD−AQ complex (kJ/mol) |
|---|---|---|---|---|
| 1 | 115 ± 9 | 4.7 ± 0.4 | $(2.2 \pm 0.2) \times 10^1$ | −7.7 ± 0.3 |
| 2 | 100 ± 8 | 4.7 ± 0.4 | $(3.0 \pm 0.3) \times 10^1$ | −8.4 ± 0.3 |
| 3 | 94 ± 8 | 4.7 ± 0.4 | $(4.5 \pm 0.5) \times 10^1$ | −9.5 ± 0.3 |
| 4 | 81 ± 7 | 4.7 ± 0.4 | $(7.3 \pm 0.8) \times 10^1$ | −10.6 ± 0.3 |
| 5 | 67 ± 6 | 4.7 ± 0.4 | $(3.5 \pm 0.4) \times 10^1$ | −14.5 ± 0.3 |
| 6 | 31 ± 3 | 4.7 ± 0.4 | $(3.2 \pm 0.4) \times 10^1$ | −20.0 ± 0.3 |

[a]Equal to the average number of bound MHA ligands per QD listed in Table 1. [b]Extracted from a global fit of the data in Figure 3B with eq 4, where $\lambda_{max}$ is shared among all six data sets. The error bars are fitting errors. [c]Errors are propagated from the errors in $K_a$ using the method described in the Supporting Information.

$$K^o = \frac{\alpha_{[PbS\ QD-AQ]}}{\alpha_{[PbS\ QD]} \times a_{[AQ]}} = \frac{\gamma_{[PbS\ QD-AQ]}}{\gamma_{[PbS\ QD]} \times \gamma_{[AQ]}} \times \frac{C_{[PbS\ QD-AQ]}}{C_{[PbS\ QD]} \times C_{[AQ]}} \times C^o \approx K_a \times C^o \tag{5a}$$

$$\Delta G_{obs} = -RT\ln\ K^o \tag{5b}$$

a dimensionless equilibrium constant, $K^o$, and then into the total Gibbs free energy change for the QD−AQ adsorption reaction, $\Delta G_{obs}$, and list these values in Table 2. In eqs 5a and 5b, $\alpha$, $r$, and $C$ are the activity, activity coefficient, and concentration, respectively, of the species indicated in the bracket; $C^o$ is the standard concentration (1 M) of solution that we apply to cancel out the units of concentration when converting concentration to activity; $R$ is the ideal gas constant (8.314 J/(mol·K)), and $T$ = 298 K.

**An Electrostatic Double-Layer Model for the Influence of Interfacial Charge Density on $\Delta G_{obs}$.** Finally, we develop a model to predict the observed free energy of adsorption for the QD−AQ complex, which includes permeation of the charged ligand shell and adsorption of AQ to the QD surface, from the number of charged ligands on the QD surface. We first approximate that the negative charges at the MHA/solvent interface surrounding a QD create a spherically symmetric electric field that results in a concentration of counterions (here, $Na^+$, $H^+$) that is larger than their concentration in bulk solution, and a concentration of co-ions (AQ, $OH^-$ and free MHA) that is smaller than their concentration in bulk solution. The concentration of AQ is therefore not uniform as it would be in an ideal solution and is instead better described by an electrostatic double-layer model[47] using the Boltzmann distribution, eq 6. In eq 6, $n(r)$ is the concentration of AQ located at a distance $r$ from the center of QD:

$$n(r) = n(\infty)\exp\left(\frac{-N_A e\varphi(r)}{RT}\right) \tag{6}$$

where $n(\infty)$ is the concentration of AQ in the bulk solution (infinitely far away from the charged $-COO^-$ groups on the surface of QD); $N_A$ is Avogadro's number ($6.022 \times 10^{23}$/mol); $e$ is the elementary charge ($1.6 \times 10^{-19}$ C); and $\varphi(r)$ is the electrostatic potential at distance $r$ from the center of QD. The concentration of AQ decays with decreasing distance from the QD core due to increasing Coulomb repulsion (i.e., increasing $\varphi(r)$). Eq 6 can be rationalized further by the concept of electrochemical equilibrium, which is explained in detail in the Supporting Information, eqs S4−S8. We then define the Gibbs free energy change upon translation of an AQ from bulk solution to the surface of a QD (located at $r_{core}$ = the radius of the QD core, 1.6 nm), $\Delta G_{trans}$, using eq 7:

$$\Delta G_{trans} = -RT\ \ln\left(\frac{n(r_{core})}{n(\infty)}\right) = N_A e\varphi(r_{core}) \tag{7}$$

If, for simplicity, we assume that the presence of charged ligands only affects the translation of AQ to the QD surface and does not influence the binding affinity between QD and AQ once it reaches the QD surface, then the observed free energy change, $\Delta G_{obs}$, listed in Table 2, is a sum of $\Delta G_{trans}$ (eq 7), which varies with surface charge density of the QD, and $\Delta G_{ads}$, the free energy change upon adsorption of an AQ to a *neutral* QD, which does not vary with surface charge density of the


DOI: 10.1021/jacs.6b03970
J. Am. Chem. Soc. 2016, 138, 8847−8854

QD. This simplification is useful because it allows us to assign the same value of $\Delta G_{ads}$ to all six samples with different surface compositions, and to define $\Delta G_{obs}$ with eq 8:

$$\Delta G_{obs} = \Delta G_{ads} + \Delta G_{trans} = \Delta G_{ads} + N_A e\varphi(r_{core}) \quad (8)$$

In this model, the increasingly negative values of $\Delta G_{obs}$ with decreasing surface charge are caused by decreasing $\varphi(r_{core})$.

We then define the relationship between $\varphi(r_{core})$ in eq 8 and the average number of bound MHA per QD, $x$, quantified with $^1$H NMR. Here we note the fact that, for MHA, the p$K_a$ of the −COOH tail group may increase at high coverages of MHA due to the increased energetic cost of abstracting a proton in a region of high local density of negative charges.[34] The presence of $Na^+$, however, partially offsets these repulsive interactions, and the pH of the QD dispersions that we investigated, 9.6−10.3, will provide the basic condition necessary to deprotonate the majority, if not all, of these protons. We therefore make the approximation that all −COOH groups on the QD surface are deprotonated at pH ≈ 10, and that each MHA ligand contributes one negative charge to the QD ligand shell.

Calculation of $\varphi(r_{core})$ requires a solution of Poisson−Boltzmann equation[48] that includes a difficult measurement or computation of the distribution of counterions as an input parameter. Instead of searching for an exact solution for $\varphi(r_{core})$, we approximate that addition of each MHA ligand increases $\varphi(r_{core})$ by $\varphi_0$, eq 9:

$$\varphi_0 = A \times \frac{e}{4\pi\varepsilon_r\varepsilon_0 r_{core}} \quad (9)$$

In eq 9, $\varepsilon_r$ is the relative permittivity of the medium, $\varepsilon_0$ is the vacuum permittivity, and $A$ is a shared empirical prefactor ($0 < A < 1$) we use to account for the screening effects from counterions in solution. In using this model, we assume that the electric field close to a QD surface with $x$ MHA ligands can be approximated as a spherically symmetric field that generates a potential defined by eq 10. Combining eqs 8 and 10, we obtain an expression for $\Delta G_{obs}$, eq 11:

$$\varphi(r_{core}) = x \times \varphi_0 = A \times \frac{xe}{4\pi\varepsilon_r\varepsilon_0 r_{core}} \quad (10)$$

$$\Delta G_{obs} = \Delta G_{ads} + N_A e \times A \times \frac{xe}{4\pi\varepsilon_r\varepsilon_0 r_{core}} = \Delta G_{ads} + mx \quad (11)$$

Figure 5 shows a plot of $\Delta G_{obs}$ (listed in Table 2) vs the mean number of MHA ligands bound per QD (listed in Table 1). We fit these data with eq 11, and the good fit ($R^2$ = 0.95) implies

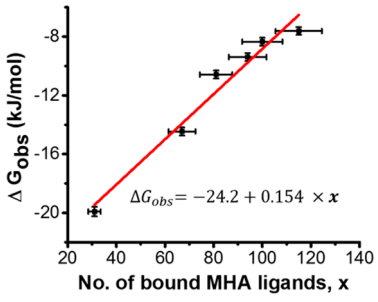


**Figure 5.** Plot of observable Gibbs free energy change, $\Delta G_{obs}$ (listed in Table 2), as a function of the average number of bound MHA per PbS QD (listed in Table 1). The red line is a fit of these data using eq 11. The $y$-intercept, −24.2 kJ/mol, equals $\Delta G_{ads}$.

that $\Delta G_{obs}$ is well-described by the proposed electrostatic double-layer model. By introducing each additional MHA to the ligand shell, we make the driving force for translation, $\Delta G_{trans}$, more positive (more unfavorable) and make $\Delta G_{obs}$ less negative by ∼154 J/mol. Fit of the data yields a value for $\Delta G_{ads}$, the adsorption constant for the neutral QD−AQ complex, of ∼ −24.2 kJ/mol, which translates into an adsorption equilibrium constant, $K_a$, of $1.7 \times 10^4$ $M^{-1}$. This number agrees with the previously reported values for QD−molecule complexes in the weak binding regime.[15,41,49−53]

## CONCLUSIONS

We fabricated a series of water-soluble PbS QDs capped by mixed monolayers of charged mercaptohexanoate and neutral mercaptohexanol, with a controllable interfacial charge density, and quantified the permeability of these monolayers to a charged small-molecule, a sulfonate-functionalized anthraquinone, using photoinduced eT between the QD and the anthraquinone as a probe of their interaction. NMR spectroscopy enabled quantification of charge density on the QD surface, and steady-state PL spectroscopy and ultrafast transient absorption spectroscopy enabled measurement of the rate and yield of photoinduced eT. A thermodynamic electrostatic double-layer model satisfactorily described the influence of the local electric field generated by these charged ligands on the free energy for transfer of the charged anthraquinone to the surface of the QD and thereby mapped the charge density at the QD/solvent interface to the redox activity of the QD. This model yielded a value for the change in driving force for the formation of the QD−molecule complex upon introduction of each additional charged ligand into the ligand shell (154 J/mol) and the value for the adsorption constant of the QD−molecule complex in the absence of electrostatic interactions (−24.2 kJ/mol).

Our simple electrostatic double-layer model fits the data and yields quantitative information about electrostatic interactions on the nanoscale that are difficult to determine using other methods, but it has some limitations, namely (i) the treatment of excess counterions ($Na^+$) as a constant screening background, which is inaccurate in the low-concentration limit according to the theoretical predictions by Szleifer and coworkers;[34] and (ii) the approximation that the charged ligands are evenly distributed on the surface of the QD and create a uniform, spherically symmetric electrostatic field. At low coverages of MHA ligands, the van der Waals interactions among the alkyl chains may compete with electrostatic repulsions and cause ligands to form bundles.[47,54,55] Additionally, the model predicts a single, presumably average, adsorption constant for the QD/AQ system, whereas there are several possible binding geometries (for example, through sulfonate group, through the oxygen lone pair, or through the pi system of AQ). We believe that the photoinduced eT yield, as measured by the PL of the samples in the presence of AQ, is a sensitive enough probe of these interactions to warrant a model that treats both the QD surface and the ionic species in solution with molecular-level detail.

This work bridges the classic models of colloid chemistry[46] with the observable electronic processes of QDs and provides us with an insight into the versatility of surface chemistry in controlling the optical properties of QDs exposed to various potential adsorbates. Our results once again[12,14,15,23,53,56] demonstrate the sensitivity of photoinduced charge transfer as a probe of not only the local chemical environment of a


DOI: 10.1021/jacs.6b03970
J. Am. Chem. Soc. 2016, 138, 8847−8854

colloid but also the intermolecular structure of its surfactant layer, which is difficult to characterize using traditional analytical tools. By embedding electrostatic interactions within QD-molecule assemblies, we could construct a highly selective recognition/reaction platform for ionic species based on their charges, and the use of water as the medium for this system makes these results an exciting step toward potential applications of water-soluble QDs in biological imaging, environmental sensing, and photocatalysis.

## ■ ASSOCIATED CONTENT

### Supporting Information

The Supporting Information is available free of charge on the ACS Publications website at DOI: 10.1021/jacs.6b03970.

Details of QD synthesis, QD size measurements (transmission electron microscopy and UV−Vis spectroscopy); $^1$H NMR spectra for MHA/MHO mixed-monolayer ligand shell quantification; cyclic voltammetry, photochemistry, and UV−Vis ground-state absorption study for AQ; time-dependent study for PL quenching experiments; ultrafast and microsecond time scale TA kinetics and the corresponding PL spectra; calculations of experimental errors; conversion of no. of bound MHA ligands to interfacial charge density; derivation of eq 6 (PDF)

## ■ AUTHOR INFORMATION


### Corresponding Author

*e-weiss@northwestern.edu


### Notes

The authors declare no competing financial interest.

## ■ ACKNOWLEDGMENTS

This work was supported by the National Science Foundation (award no. 1400596) to E.A.W. C.H. thanks the Hierarchical Materials Cluster Program (HMCP), supported by The Graduate School at Northwestern University, for a fellowship. NMR measurements were performed at Northwestern University's Integrated Molecular Structure Education and Research Center (IMSERC) with the assistance of Dr. Yuyang Wu and Dr. Yongbo Zhang. Transmission electron microscopy was performed at the NUANCE Center, Northwestern University, with the help of Dr. Dmitriy Dolzhnikov. NUANCE is supported by the International Institute for Nanotechnology, the Northwestern Materials Research Science and Engineering Center (MRSEC, NSF DMR 1121262), the Keck Foundation, the State of Illinois, and Northwestern University.

## ■ REFERENCES


(1) Hetsch, F.; Zhao, N.; Kershaw, S. V.; Rogach, A. L. *Mater. Today* **2013**, *16*, 312−325.
(2) Talapin, D. V.; Murray, C. B. *Science* **2005**, *310*, 86−89.
(3) Nozik, A. J.; Beard, M. C.; Luther, J. M.; Law, M.; Ellingson, R. J.; Johnson, J. C. *Chem. Rev.* **2010**, *110*, 6873−90.
(4) Kamat, P. V. *J. Phys. Chem. C* **2008**, *112*, 18737−18753.
(5) Wu, K.; Zhu, H.; Lian, T. *Acc. Chem. Res.* **2015**, *48*, 851−859.
(6) Jensen, S. C.; Bettis Homan, S.; Weiss, E. A. *J. Am. Chem. Soc.* **2016**, *138*, 1591−1600.
(7) Bruchez, M., Jr.; Moronne, M.; Gin, P.; Weiss, S.; Alivisatos, A. P. *Science* **1998**, *281*, 2013−2016.
(8) Mattoussi, H.; Mauro, J. M.; Goldman, E. R.; Anderson, G. P.; Sundar, V. C.; Mikulec, F. V.; Bawendi, M. G. *J. Am. Chem. Soc.* **2000**, *122*, 12142−12150.
(9) Chan, W. C. W.; Nie, S. *Science* **1998**, *281*, 2016−2018.
(10) Love, J. C.; Estroff, L. A.; Kriebel, J. K.; Nuzzo, R. G.; Whitesides, G. M. *Chem. Rev.* **2005**, *105*, 1103−1170.
(11) Whitesides, G. M.; Laibinis, P. E. *Langmuir* **1990**, *6*, 87−96.
(12) Knowles, K. E.; Malicki, M.; Weiss, E. A. *J. Am. Chem. Soc.* **2012**, *134*, 12470−3.
(13) Knowles, K. E.; Peterson, M. D.; McPhail, M. R.; Weiss, E. A. *J. Phys. Chem. C* **2013**, *117*, 10229−10243.
(14) Knowles, K. E.; Tagliazucchi, M.; Malicki, M.; Swenson, N. K.; Weiss, E. A. *J. Phys. Chem. C* **2013**, *117*, 15849−15857.
(15) Malicki, M.; Knowles, K. E.; Weiss, E. A. *Chem. Commun.* **2013**, *49*, 4400−2.
(16) Degefa, T. H.; Schön, P.; Bongard, D.; Walder, L. *J. Electroanal. Chem.* **2004**, *574*, 49−62.
(17) Benítez, G.; Vericat, C.; Tanco, S.; Remes Lenicov, F.; Castez, M. F.; Vela, M. E.; Salvarezza, R. C. *Langmuir* **2004**, *20*, 5030−5037.
(18) Campiña, J. M.; Martins, A.; Silva, F. *J. Phys. Chem. C* **2007**, *111*, 5351−5362.
(19) Ku, J.-R.; Lai, S.-M.; Ileri, N.; Ramírez, P.; Mafé, S.; Stroeve, P. *J. Phys. Chem. C* **2007**, *111*, 2965−2973.
(20) Lee, S. B.; Martin, C. R. *Anal. Chem.* **2001**, *73*, 768−775.
(21) Aruda, K. O.; Bohlmann Kunz, M.; Tagliazucchi, M.; Weiss, E. A. *J. Phys. Chem. Lett.* **2015**, *6*, 2841−2846.
(22) Peterson, M. D.; Jensen, S. C.; Weinberg, D. J.; Weiss, E. A. *ACS Nano* **2014**, *8*, 2826−2837.
(23) Boldt, K.; Jander, S.; Hoppe, K.; Weller, H. *ACS Nano* **2011**, *5*, 8115−8123.
(24) Boulesbaa, A.; Issac, A.; Stockwell, D.; Huang, Z.; Huang, J.; Guo, J.; Lian, T. *J. Am. Chem. Soc.* **2007**, *129*, 15132−15133.
(25) Song, N.; Zhu, H.; Jin, S.; Zhan, W.; Lian, T. *ACS Nano* **2011**, *5*, 613−621.
(26) Vinayakan, R.; Shanmugapriya, T.; Nair, P. V.; Ramamurthy, P.; Thomas, K. G. *J. Phys. Chem. C* **2007**, *111*, 10146−10149.
(27) Eckermann, A. L.; Feld, D. J.; Shaw, J. A.; Meade, T. J. *Coord. Chem. Rev.* **2010**, *254*, 1769−1802.
(28) Hickman, J. J.; Ofer, D.; Zou, C.; Wrighton, M. S.; Laibinis, P. E.; Whitesides, G. M. *J. Am. Chem. Soc.* **1991**, *113*, 1128−1132.
(29) Moreels, I.; Lambert, K.; Smeets, D.; De Muynck, D.; Nollet, T.; Martins, J. C.; Vanhaecke, F.; Vantomme, A.; Delerue, C.; Allan, G.; Hens, Z. *ACS Nano* **2009**, *3*, 3023−3030.
(30) Hines, M. A.; Scholes, G. D. *Adv. Mater.* **2003**, *15*, 1844−1849.
(31) Hyun, B.-R.; Chen; Rey, D. A.; Wise, F. W.; Batt, C. A. *J. Phys. Chem. B* **2007**, *111*, 5726−5730.
(32) Kalsin, A. M.; Kowalczyk, B.; Wesson, P.; Paszewski, M.; Grzybowski, B. A. *J. Am. Chem. Soc.* **2007**, *129*, 6664−6665.
(33) McMurry, J. E. *Organic Chemistry*, 8th ed.; Cengage Learning: Belmont, CA, 2012.
(34) Wang, D.; Nap, R. J.; Lagzi, I.; Kowalczyk, B.; Han, S.; Grzybowski, B. A.; Szleifer, I. *J. Am. Chem. Soc.* **2011**, *133*, 2192−2197.
(35) Hens, Z.; Martins, J. C. *Chem. Mater.* **2013**, *25*, 1211−1221.
(36) Morris-Cohen, A. J.; Malicki, M.; Peterson, M. D.; Slavin, J. W. J.; Weiss, E. A. *Chem. Mater.* **2013**, *25*, 1155−1165.
(37) Jasieniak, J.; Califano, M.; Watkins, S. E. *ACS Nano* **2011**, *5*, 5888−5902.
(38) Wu, K.; Liang, G.; Shang, Q.; Ren, Y.; Kong, D.; Lian, T. *J. Am. Chem. Soc.* **2015**, *137*, 12792−12795.
(39) Zhu, H.; Song, N.; Lian, T. *J. Am. Chem. Soc.* **2010**, *132*, 15038−15045.
(40) Zhu, H.; Song, N.; Rodríguez-Córdoba, W.; Lian, T. *J. Am. Chem. Soc.* **2012**, *134*, 4250−4257.
(41) Morris-Cohen, A. J.; Frederick, M. T.; Cass, L. C.; Weiss, E. A. *J. Am. Chem. Soc.* **2011**, *133*, 10146−54.
(42) Huang, J.; Huang, Z.; Yang, Y.; Zhu, H.; Lian, T. *J. Am. Chem. Soc.* **2010**, *132*, 4858−4864.
(43) Yang, Y.; Rodríguez-Córdoba, W.; Lian, T. *Nano Lett.* **2012**, *12*, 4235−4241.
(44) Ding, T. X.; Olshansky, J. H.; Leone, S. R.; Alivisatos, A. P. *J. Am. Chem. Soc.* **2015**, *137*, 2021−2029.




DOI: 10.1021/jacs.6b03970
*J. Am. Chem. Soc.* 2016, 138, 8847−8854

(45) Matylitsky, V. V.; Dworak, L.; Breus, V. V.; Basché, T.; Wachtveitl, J. *J. Am. Chem. Soc.* **2009**, *131*, 2424−2425.
(46) Atkins, P. W. *Physical Chemistry*, 9th ed.; W.H. Freeman: New York, 2010.
(47) Walker, D. A.; Kowalczyk, B.; de la Cruz, M. O.; Grzybowski, B. A. *Nanoscale* **2011**, *3*, 1316−1344.
(48) Fogolari, F.; Brigo, A.; Molinari, H. *J. Mol. Recognit.* **2002**, *15*, 377−392.
(49) Donakowski, M. D.; Godbe, J. M.; Sknepnek, R.; Knowles, K. E.; Olvera de la Cruz, M.; Weiss, E. A. *J. Phys. Chem. C* **2010**, *114*, 22526−22534.
(50) Ji, X.; Copenhaver, D.; Sichmeller, C.; Peng, X. *J. Am. Chem. Soc.* **2008**, *130*, 5726−5735.
(51) Moreels, I.; Martins, J. C.; Hens, Z. *ChemPhysChem* **2006**, *7*, 1028−1031.
(52) Moreels, I.; Martins, J. C.; Hens, Z. *Sens. Actuators, B* **2007**, *126*, 283−288.
(53) Morris-Cohen, A. J.; Vasilenko, V.; Amin, V. A.; Reuter, M. G.; Weiss, E. A. *ACS Nano* **2012**, *6*, 557−565.
(54) Guo, P.; Sknepnek, R.; Olvera de la Cruz, M. *J. Phys. Chem. C* **2011**, *115*, 6484−6490.
(55) Sandberg, D. J.; Carrillo, J.-M. Y.; Dobrynin, A. V. *Langmuir* **2007**, *23*, 12716−12728.
(56) Weinberg, D. J.; He, C.; Weiss, E. A. *J. Am. Chem. Soc.* **2016**, *138*, 2319−26.


DOI: 10.1021/jacs.6b03970
*J. Am. Chem. Soc.* 2016, 138, 8847−8854